

Article

Solar Light-Induced Photocatalytic Response of BiOCl/PANI Composite towards the Degradation of Tetracycline

Janis Goyal [†], Surbhi Sharma [†]  and Soumen Basu ^{*†} 

School of Chemistry and Biochemistry, Thapar Institute of Engineering & Technology, Patiala 147004, India

^{*} Correspondence: soumen.basu@thapar.edu or sbasu1980@gmail.com[†] These authors contributed equally to this work.

Abstract: Photocatalytic degradation has gained much attention as a means of reducing water contamination as, with increasing industrialization and population growth, water pollution is a menace to both individuals and the environment. In this respect, metal oxide photocatalysts demonstrate effectiveness due to their excellent properties, such as their narrow band gap and low recombination rate of charge carriers. Here, various weight ratios of BiOCl/PANI composites have been synthesized by the simple wet chemical method. The crystallinity, oxidation state and surface chemical composition of the elements were analyzed by XRD and XPS techniques. FESEM and HRTEM images verified the formation of BiOCl nanosheets, covered well with PANI nanofibers, while EDX spectra revealed the uniform distribution of elements. The high surface area of the photocatalyst with a mesoporous nature was revealed by BET analysis. Low recombination rate and narrow band gap, suitable for photocatalysis, were confirmed by PL and UV-DRS spectroscopy. The photocatalytic performance of the photocatalyst was tested for the photodegradation of rhodamine-B (Rh-B) and tetracycline (TC) under natural sunlight irradiation. Kinetic results demonstrated that the 15% BiOCl/PANI hybrid exhibits excellent photocatalytic activity, degrading 97% of Rh-B and 77% of TC with a high rate constant (for Rh-B 0.0236 min^{-1} and for TC 0.0106 min^{-1}). Trapping experiments highlighted that $\text{O}_2^{\bullet-}$ radicals play a vital role in the photodegradation mechanism. The reusability studies confirmed the good stability of the catalyst for the degradation of Rh-B (~85%) after five sequential runs. Considering its superior properties and ease of preparation, the synthesized photocatalyst can be used for ecological remediation.



Citation: Goyal, J.; Sharma, S.; Basu, S. Solar Light-Induced Photocatalytic Response of BiOCl/PANI Composite towards the Degradation of Tetracycline. *Catalysts* **2023**, *13*, 795. <https://doi.org/10.3390/catal13050795>

Academic Editors: Rosanna Pagano, Ludovico Valli and Zois Syrgiannis

Received: 17 March 2023

Revised: 15 April 2023

Accepted: 21 April 2023

Published: 24 April 2023



Copyright: © 2023 by the authors. Licensee MDPI, Basel, Switzerland. This article is an open access article distributed under the terms and conditions of the Creative Commons Attribution (CC BY) license (<https://creativecommons.org/licenses/by/4.0/>).

Keywords: PANI/BiOCl; photodegradation; tetracycline; wastewater treatment; sunlight

1. Introduction

Nearly two-thirds of Earth's is occupied by water; however, due to unceasingly increasing population growth and global industrialization, the shortage of pure and clean water has long been a challenge for humanity on a global scale [1–3]. Industrial effluents and coloring agents such as dyes, pesticides, microplastics and pharmaceuticals from industries, medical organizations and domestic areas, grievously affect mankind and aquatic regions, as these are extremely toxic, disastrous, carcinogenic and not easy to degrade [4,5]. It is estimated that over 10,000 tons of dyes are expected to be produced annually and around 20% of this waste is discharged into the environment [6,7]. In addition to dyes, colorless phenolic compounds and pharmaceuticals, particularly antibiotics, are toxic pollutants in water bodies [2,8]. Most antibiotics, including tetracycline, are expelled through urine and feces as the original parent component as they are poorly digested [9]. Pharmaceuticals are present in surface water and wastewater treatment areas, discharged in unavoidable concentrations of ng L^{-1} to $\mu\text{g L}^{-1}$, and both their presence and persistence in surface waters are detrimental [8,10]. Therefore, it is crucial to properly treat wastewater before releasing it to maintain our ecosystem. Tetracycline (TC) is a highly detectable broad-spectrum antibiotic that has been widely utilized in both human and veterinary medicine

to cure and reduce the risk of developing infections [11–13]. TC cannot adequately be adsorbed by the digestive tracts of both humans and animals, and it is suggested that between 50–80% is excreted either through feces or urine [9]. Studies on the environmental monitoring of TC demonstrate that considerable levels (100–500 mg/L) of TC were found in hospital and pharmaceutical sector wastewater effluents [14].

Rhodamine B (Rh-B) is a water-soluble, toxic, cationic, fluorescent xanthene dye that is widely used as a dyeing agent in textile industries [15,16]. It is known to exhibit long-lasting neurotoxic effects. Rh-B exposure can cause nausea, skin problems, nasal irritation, eye allergies, gastrointestinal disorders, development disorders and neurological and reproductive toxicity [17,18]. Therefore, it is crucial to explore its effective removal strategies from water systems.

Several strategies have been tried in attempts to eliminate persistent pollutants released into aquatic life such as adsorption, coagulation, filtration, ion exchange, extraction, sedimentation and electrochemical process [19–21]. However, that these processes are time-consuming, not cost-effective and need proper maintenance of physical conditions such as temperature/pressure limits their practical applications. Furthermore, these methods do not promise total eradication and can cause secondary pollution, which will require further treatment [22,23]. Semiconductor photocatalysis has been known to be an effective method to eradicate organic pollutants as it is economical, environmentally friendly, and quite effective for the degradation of harmful pollutants by utilizing natural sunlight [24,25]. It ensures the complete degradation of harmful contaminants by converting them into CO₂, H₂O and minerals without causing secondary pollution [23,26]. Among various semiconducting materials, BiOCl exhibits strong photocatalytic activity with good optoelectronic properties. BiOCl is an excellent non-toxic, corrosion-resistant catalyst, with high redox ability and an indirect transmission energy gap [27,28]. The photocatalytic activity of BiOCl is due to the existence of a uniquely layered structure in which [Bi₂O₂]²⁺ layers stacked between two Cl ions account for low the recombination of charge carriers. BiOCl's broad band gap of approximately 3.2–3.6 eV restricts its applicability because it can be stimulated by ultraviolet light only [29]. To improve the photocatalytic performance of BiOCl in natural light, doping of BiOCl with a conducting polymer with low band gap to form an efficient heterojunction catalyst is an excellent option in the aspect of degradation [1]. Conducting polymers with conjugated electron systems and transition metal oxide composites possess substantial improvement in their photocatalytic activity [30,31]. Due to different charge carrier recombination delays, the hybrid material contains a strong photo response with a wide surface area for the absorption of light [30]. The conducting polymer, polyaniline (PANI), has drawn much attention in the field of photocatalysis as it possesses a wide range of applications. It can easily be synthesized by using a low-temperature chemical oxidative process [32]. PANI has a high electron–hole carrying capacity due to which it is mixed with oxides of transition metal nanoparticles in order to improve their photocatalytic properties for organic dye decomposition and the purification of water. It acts as an excellent carrier of electrons as well as holes throughout its chain due to the presence of unique linear chain benzene rings, which are connected through nitrogen atoms [33].

Recently, several novel materials have being reported for the purpose of pollutant-degradation. Tang et al. [34] fabricated BiPO₄/Oxygen vacancy-rich-BiOBr heterojunction composite via a solvothermal route for the TC-degradation. Xie et al. [35] synthesized a series of 0D/2D TiO₂ nanoparticles/Bi₂O₃ nanosheet heterojunctions through a sol-gel method followed by ultrasonication. This material was then utilized for the TC degradation under visible light and a maximum of 0.1443 min⁻¹ rate constant was accomplished. The synthesis of Fe₂O₃/bentonite/TiO₂ was conducted by Al-Musawi et al. [36], and ~98.8% degradation of amoxicillin was demonstrated under visible light with a rate constant of 0.0176 min⁻¹. A g-C₃N₄/Ag₃PO₄ composite Z-type photocatalyst was manufactured by Chen et al. [37], which was later tested for the degradation of ofloxacin and a degradation efficacy of ~71.9% in 10 min, along with a rate constant of 0.09297 min⁻¹, was obtained. Tanwar et al. synthesized PANI/Fe doped BiOCl photocatalysts using a facile chemisorp-

tion process. The synthesized product exhibits an enhanced surface area of 24.43 m²/g and exhibits good degradation efficiency for Congo red (80%) under visible light [38]. Wang et al. employed a facile chemisorption process to prepare PANI/BiOCl nanocomposites, which degrade 67% of methyl orange in 210 min in visible light [39]. Wang and Hao et al. prepared PANI/BiOCl composites with different weight ratios via the hydrothermal method and, thereafter, photodegradation efficiency was scrutinized for the degradation of Rhodamine-B in visible light illumination [40]. The BiOCl/PANI combination has been used to degrade several dyes in the past; however, its application for pharmaceutical degradation in sunlight has not gained much attention.

The present work focuses on the synthesis of PANI/BiOCl nanocomposite by employing simple sonication and centrifugation process and, thereafter, investigating photodegradation efficiency for colored Rh-B and, for comparison, colorless pharmaceutical TC under natural sunlight, with a comparative study of other photocatalysts reported in the literature. The effect of different reaction parameters on degradation efficiency, such as pH and catalyst concentration were examined. To study the photodegradation mechanism and role of active photogenerated species, trapping experiments were conducted. The catalyst's reusability efficiency was also tested and characterized by XRD and FESEM analysis after five degradation cycles. To the best of the authors' knowledge, PANI/BiOCl nanocomposites have not been used for the degradation of colorless pharmaceutical Tetracycline under intense natural sunlight.

2. Results and Discussion

2.1. XPS Analysis

XPS technique was performed to examine the chemical nature and oxidation state of different elements of the composite. Figure 1a–f manifested the high-resolution XPS spectra of 15% BiOCl/PANI elements N 1s, C 1s, Cl 2p, Bi 4f and O 1s. Bismuth displayed two considerable peaks at a binding energy of 163.3 eV, and a second peak at 158.00 eV referred to Bi 4f_{5/2} and Bi 4f_{7/2}, indicating the existence of Bi³⁺ in BiOCl [41]. For oxygen, the binding energy peak appeared at 530.01 eV, which signifies the Bi–O bond. The peaks at 197.38 eV and 195.75 eV for Cl 1s are related to Cl 2p_{3/2} and Cl 2p_{1/2} respectively, corresponding to the chloride ion, Cl⁻, in BiOCl [29]. The two significant peaks at 405.8 eV and 398.8 eV represent the N 1s due to uncharged deprotonated imine and doped imine, respectively [42,43]. The C 1s possess two peaks at 284.5 eV and 282.7 eV, signifying the (C–C) and (C–O) moieties, respectively. The peaks ensured the presence of both polyaniline and BiOCl in the composite.

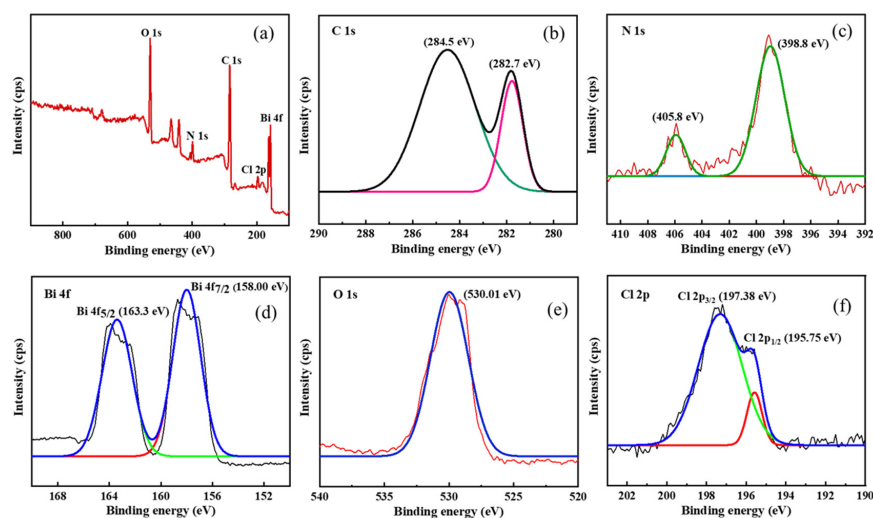


Figure 1. XPS spectra of 15% PANI/BiOCl composite: (a) survey spectrum, (b) C 1s, (c) N 1s, (d) Bi 4f, (e) O 1s and (f) Cl 2p.

2.2. XRD Analysis

The XRD patterns of BiOCl, PANI and BiOCl/PANI composites are displayed in Figure 2a. The characteristic diffraction peak positions of prepared BiOCl appeared at $2\theta \sim 12.03^\circ, 24.21^\circ, 25.81^\circ, 32.52^\circ, 33.61^\circ, 36.60^\circ, 40.90^\circ, 46.60^\circ, 49.79^\circ, 54.20^\circ, 55.19^\circ, 58.78^\circ, 67.98^\circ, 75.07^\circ,$ and 77.78° , corresponding to (001), (002), (101), (110), (102), (003), (112), (200), (113), (211), (212), (220), (310), and (310) crystalline planes of BiOCl (JCPDS No.: 06-0429) [44]. The small broad diffraction peak in the case of polyaniline signifies its amorphous nature. It has been found that the peak values of the BiOCl/PANI composite were not influenced after the formation of nanocomposite, compared with BiOCl, indicating that PANI did not disrupt the crystal lattice of BiOCl [38,45]. However, the intensities of BiOCl peaks gradually decrease on increasing PANI content due to the increased dispersivity of BiOCl [45].

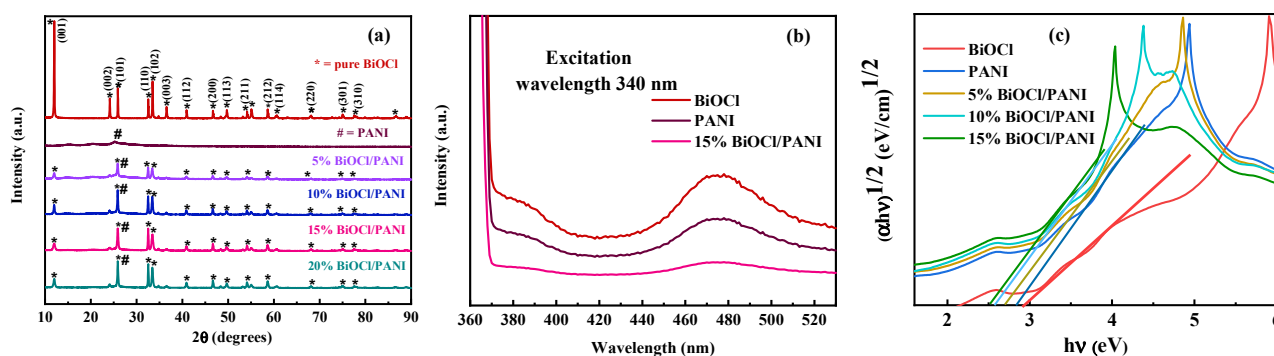


Figure 2. (a) XRD pattern, (b) PL spectra and (c) Tauc plot for prepared catalysts.

2.3. Photoluminescence Spectroscopy

The photoluminescence spectra of BiOCl and 15% BiOCl/PANI composite are expressed in Figure 2b. The photoinduced electron and hole carriers' recombination tendency and the photocatalytic performance of the material were evaluated by PL spectrum [38]. The excitation wavelength used for PANI/BiOCl composite was 340 nm. It was evident that among all that we investigated, pure BiOCl exhibited the highest PL intensity and showed an emission peak at 475 nm. The 15% BiOCl/PANI composite showed lowest PL intensity, which clearly signifies the effective high separation efficiency of photogenerated electron and hole pairs, implies the suppression in recombination of electron–hole pairs and significantly enhances the photocatalytic performance [46].

2.4. UV–Visible Diffuse Reflectance Spectroscopy

UV–visible diffuse reflectance spectroscopy (DRS) was employed to assess the band gap and optical absorbance characteristics of as-prepared photocatalysts. Tauc's plot was used to evaluate the band gap energies, followed by the Equation (1)

$$(\alpha h\nu)^{1/2} = A(h\nu - E_g), \quad (1)$$

where α , h and ν represent the absorption coefficient, Planck constant and frequency of light, respectively, and E_g represents the band gap.

From the Tauc plot (Figure 2c), it was seen that the band gap energy values for BiOCl, PANI, 5%, 10% and 15% BiOCl/PANI were $\sim 2.99, 2.82, 2.69, 2.58$ and 2.5 eV, respectively.

2.5. Nitrogen Adsorption/Desorption Analysis

The surface area of the photocatalyst is a critical parameter in photocatalysis as it significantly increases the count of active reaction sites. N_2 adsorption–desorption isotherm and BJH plot were applied to measure the active surface area and pore size distribution of the prepared catalyst, respectively, as illustrated in Figure 3a,b. All the samples correspond to type-IV isotherms and the occurrence of sharp peaks in the range of 2 nm–50 nm indicates

the mesoporous nature of the prepared composite [45]. It is observed that the BiOCl/PANI composite exhibits a larger surface area ($25 \text{ m}^2/\text{g}$) than that of BiOCl ($10 \text{ m}^2/\text{g}$) and PANI ($17 \text{ m}^2/\text{g}$), which implies that surface area is increased after the formation of the nanocomposite, as illustrated in Table 1.

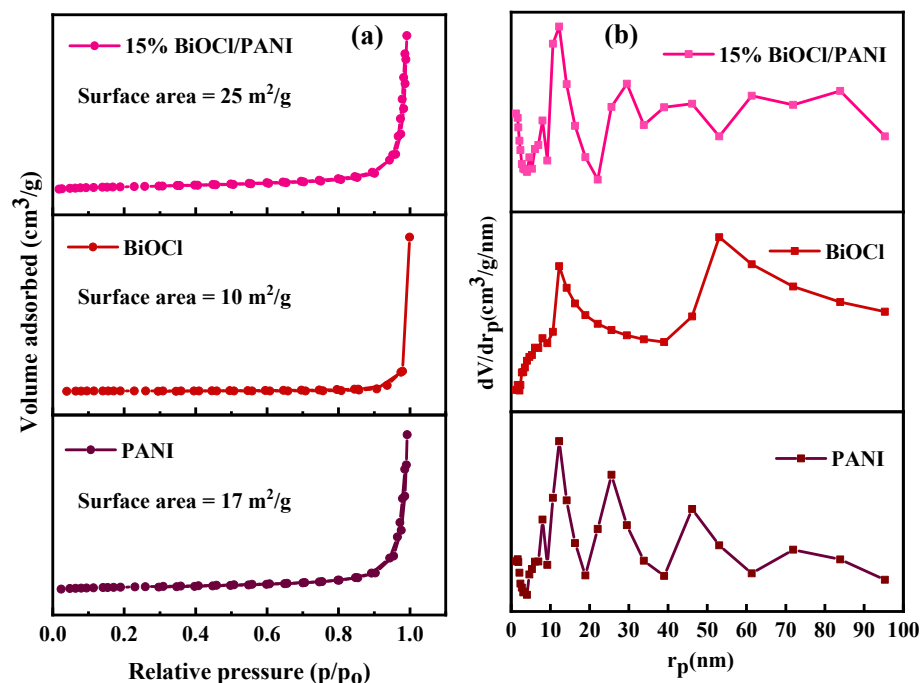


Figure 3. (a) N_2 adsorption–desorption isotherm and (b) BJH plot for as-synthesized catalysts.

Table 1. Surface properties of PANI/BiOCl photocatalyst.

Sample	Surface Area (m^2/g)	Mean Pore Diameter (nm)	Total Pore Volume (cm^3/g)
PANI	17	38.80	0.174
BiOCl	10	13.56	0.086
15% PANI/BiOCl	25	42.54	0.263

2.6. FESEM and TEM Analysis

The surface morphology of the PANI/BiOCl composite was investigated by the FESEM technique, as revealed in Figure 4. The FESEM images of BiOCl and PANI are shown in Figures 4a and 4b, respectively, while those of the composite are shown in Figure 4c,d. It is investigated that pure BiOCl appeared as large nanosheets with a smooth surface. FESEM images of the composite show that PANI consists of aggregated nanofibers, and fibrous nanoparticles of PANI well-covered the surface of the BiOCl nanosheets in the respective composite. The HRTEM images of the BiOCl/PANI composite show two different lattice fringes of BiOCl, covered with PANI on its surface, with d-space values of 0.73 \AA and 1.52 \AA , respectively, corresponding to reflection planes (001) and (114), as depicted in Figure 4e,f. This revealed the successful formation of the heterojunction structure and the heterogeneous deposition of PANI nanoparticles on BiOCl flaky sheets [44].

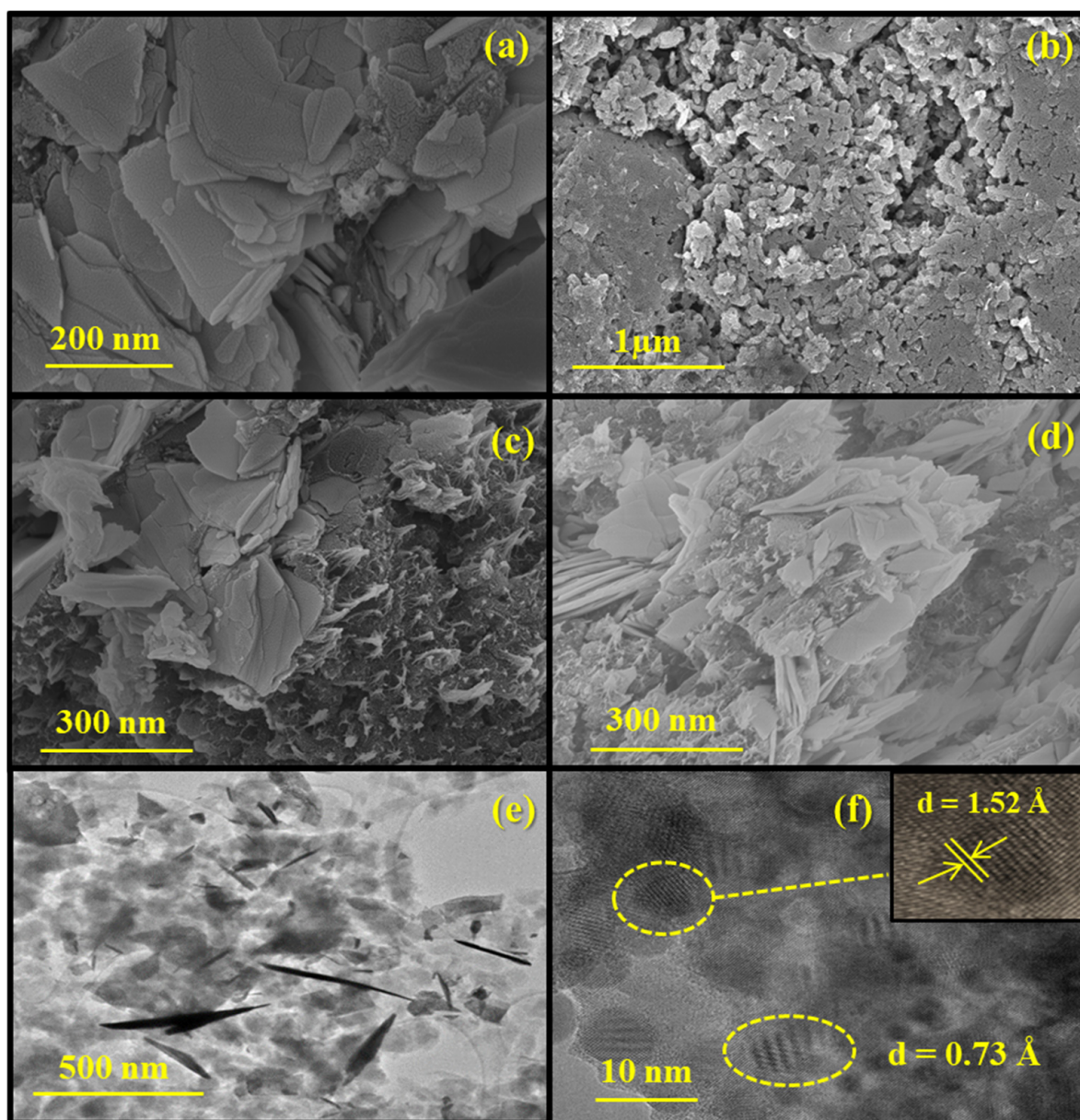


Figure 4. FESEM images of (a) BiOCl, (b) PANI, (c,d) BiOCl/PANI composite and (e,f) HRTEM images of the BiOCl/PANI composite.

2.7. EDX and Elemental Mapping

The composition of elements present in the as-synthesized catalyst was analyzed by EDS spectrum with mapping as displayed in Figure 5. It is confirmed that the composite consists of bismuth (Bi), oxygen (O), chlorine (Cl), carbon (C) and nitrogen (N) elements. The elemental mapping images demonstrated the uniform dispersal of all the elements, as displayed in Figure 5b–f.

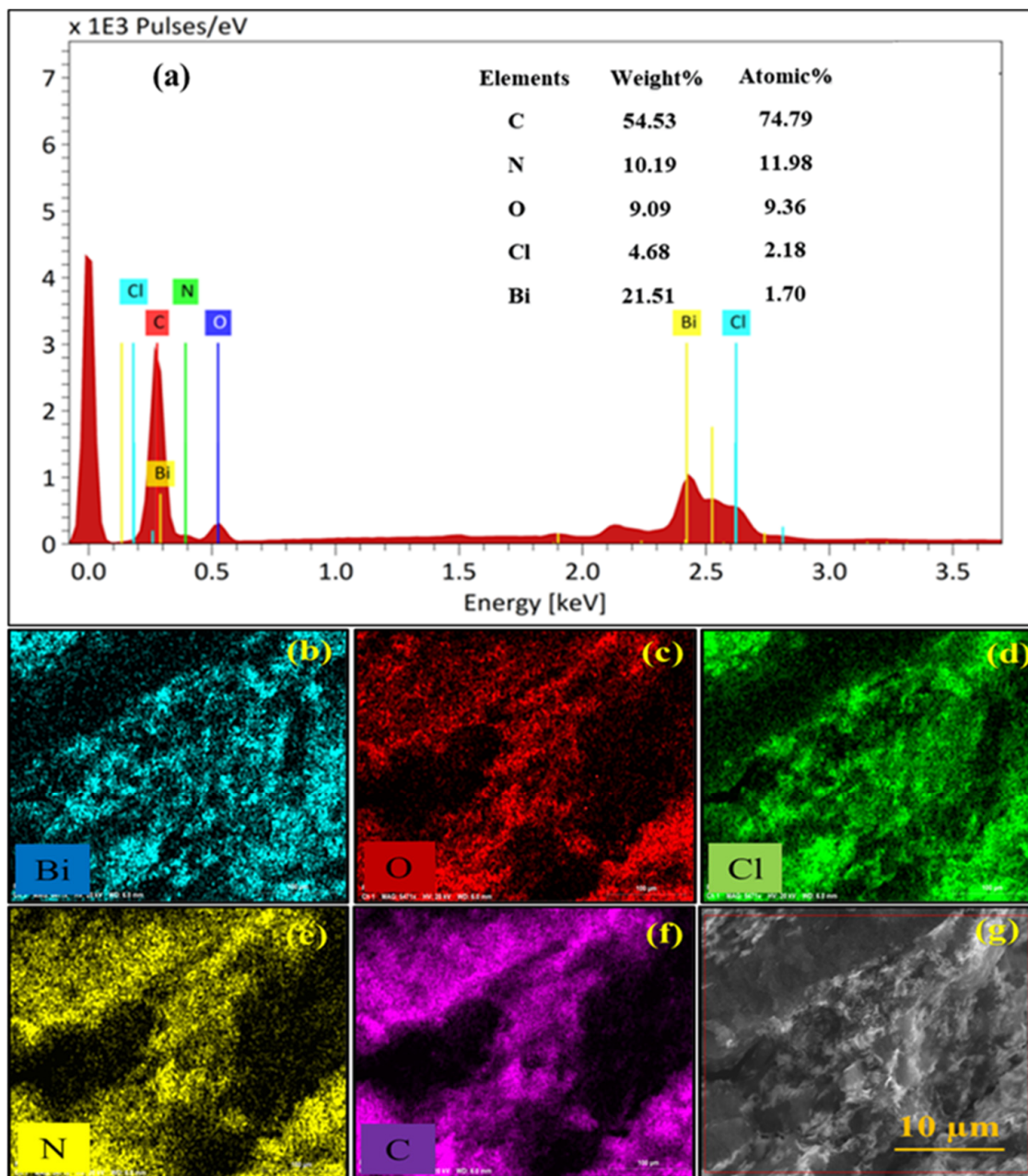


Figure 5. (a) EDX spectra of 15% PANI/BiOCl, elemental color mapping of (b) Bi, (c) O, (d) Cl, (e) N, (f) C and (g) SEM micrograph.

2.8. Photocatalytic Study

The photocatalytic activity was investigated by photodegradation of Rh-B and TC under bright sunlight. Firstly, the photodegradation of Rh-B and TC was studied without the addition of catalyst (photolysis); only 16% and 9% degradation of Rh-B and TC, respectively, were observed, as shown in Figure 6a,b. The photocatalytic degradation efficiencies of 97% (Rh-B) and 77% (TC) were found using 0.4 g/L and 0.5 g/L of catalyst.

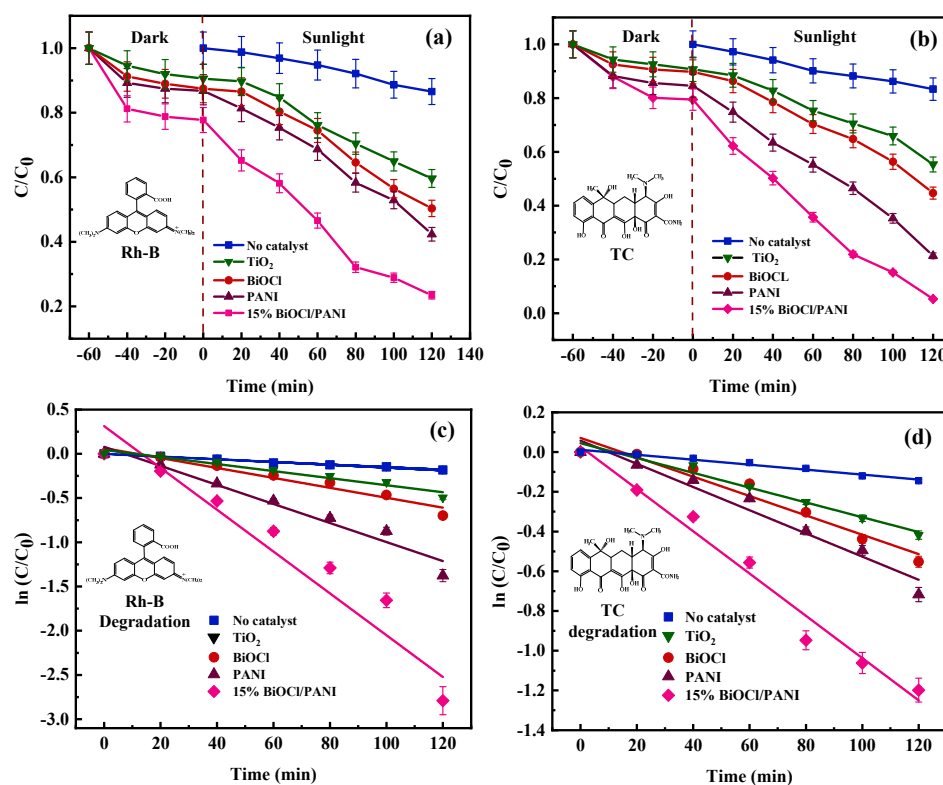


Figure 6. Kinetic study for the degradation of (a) Rh-B, (b) TC, (c) rate constant plot of Rh-B and (d) TC.

The Equation (2) was used to evaluate the rate constant:

$$\ln(C/C_0) = -kt, \quad (2)$$

where k refers to the rate constant, C_0 represents the concentration at time $t = 0$ and C represents the concentration of solution at time t .

Figure 6 represents the kinetic study of Rh-B and TC degradation. It was noted that the degradation reaction follows the pseudo-first-order reaction kinetics. The degradation activity and rate constant of as-synthesized catalysts obey the order: 15% > 10% > 5% > 20% > PANI > BiOCl > TiO₂ P25. Among various weight ratios (5%, 10%, 15% and 20% BiOCl), the 15% BiOCl/PANI composite exhibits the best removal efficiency for Rh-B and for TC from the solution under sunlight; it degraded about 97% of Rh-B in 2 h and the observed rate constant is 0.0236 min⁻¹. Similarly, the catalyst shows the highest degradation percentage of 77% for TC removal, with a rate constant of 0.0106 min⁻¹. The photocatalytic rate of the composite is even higher as compared to pure BiOCl, so further experiments were performed using the 15% PANI/BiOCl composite. The photocatalytic activity of the prepared catalyst was also compared with commercial TiO₂ P25, which degraded 45% of Rh-B and 39% of TC with rate constants of 0.0056 min⁻¹ and 0.0037 min⁻¹, respectively. The enhanced photoactivity of the composite is mainly due to the popularly known synergistic effect between PANI and BiOCl [45]. Table S1 (Supplementary file) enlists the degradation parameters of different materials towards Rh-B and TC degradation.

2.9. Effect of pH

Figure 7b illustrates the effect of pH on the photodegradation of Rh-B and TC at distinct pH values (1, 2, 3, 5, 7, 9, 10, 11). These different pH values were maintained, followed by the incorporation of HCl or NaOH (0.1 N). The results showed that photodegradation rates are slow at high and low pH for Rh-B. At natural pH, the degradation efficiencies for Rh-B and TC were 97% and 77%, respectively. The maximum degradation efficiency, in the case of Rh-B, was observed in the neutral pH range, i.e., pH = 6.51. It was observed by

measurement that the point of zero charges (pzc) for the catalyst was observed at 2.93, as demonstrated in Figure S1 (Supplementary file). The catalyst's surface contains a positive charge at $\text{pH} < 2.93$, and it becomes negatively charged at $\text{pH} > 2.93$. Rh-B is a cationic dye and, at $\text{pH} < 2.93$, it exhibits low degradation efficiency as the cationic charge on Rh-B is repelled by a positively charged photocatalyst surface. On the other hand, at $\text{pH} > 2.93$, Rh-B was absorbed properly on the catalyst's surface due to the existence of attractive interactions between positively charged dye and the negatively charged photocatalyst surface [17]. In the case of TC, degradation activity was also examined at various pH values from 1–11, and the maximum degradation percentage was observed in the neutral pH range. At $\text{pH} < 3.3$ (pKa of TC), TC is present in cationic form (TC^+); at $\text{pH} > 7.7$, it exists in anionic form (TC^-); and in between these pH values (3.3–7.7), it exists in zwitterion [9,47]. TC^+ repels the positively charged surface of the catalyst, so the degradation efficiency was decreased in this pH range. The high degradation occurs at neutral pH due to an increase in electrostatic interactions between the catalyst surface and TC. Above this range, degradation efficiency tends to decrease due to the existence of repulsive interactions between the catalyst surface and TC^- [47,48].

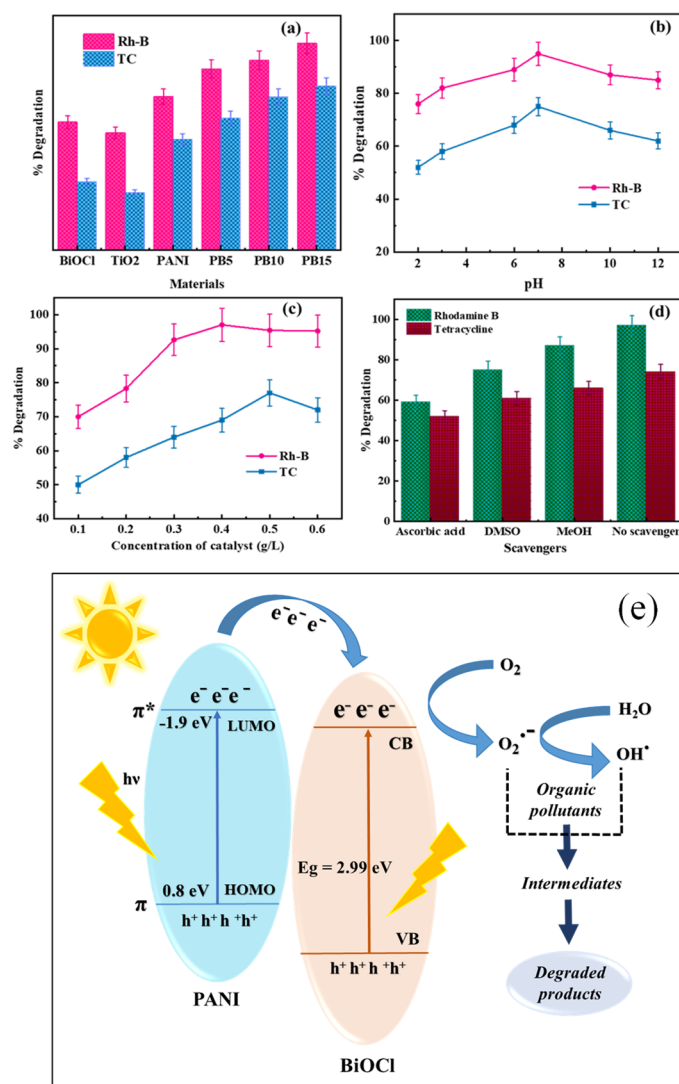


Figure 7. Plot showing (a) the comparison of degradation efficiencies of different materials, (b) effect of pH, (c) catalyst concentration, (d) scavengers on degradation efficiency of Rh-B and TC and (e) photodegradation mechanism using the PANI/BiOCl composite.

2.10. Effect of Catalyst Concentration

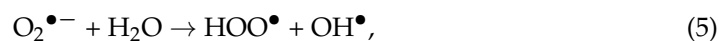
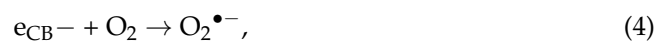
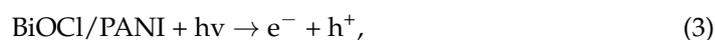
The effect of the concentration of the photocatalyst on photodegradation rate was evaluated by varying the concentrations of 15% PANI/BiOCl hybrid (0.2 g/L to 0.6 g/L), manifested in Figure 7c. It was demonstrated that the degradation efficiency considerably increases when the catalyst concentration increases from 0.2 g/L to 0.4 g/L for Rh-B. However, as the concentration reaches 0.5 g/L, saturation almost occurs. Hence, the removal efficiency for Rh-B is higher at 0.4 g/L, and for TC, it is higher at 0.5g/L. The decrease in degradation efficiency is due to the blockage of active photolytic surface sites of the catalyst due to the adsorption of pollutants which inhibit the active species formation required for photodegradation [45].

2.11. Plausible Mechanism

A trapping experiment was conducted to determine the necessity of photogenerated active radical species in the photodegradation reaction and photodegradation mechanism for Rh-B and TC under sunlight by employing a photocatalyst. Different scavengers were used in this typical experiment, such as ascorbic acid, methanol and DMSO, for trapping superoxide radicals ($O_2^{\bullet-}$), holes (h^+) and hydroxyl radicals (OH^{\bullet}), respectively, as indicated in Figure 7d [49]. It is noted after the photocatalytic experiment that the photodegradation of Rh-B and TC was substantially influenced by the addition of ascorbic acid (superoxide radical trapper). This implies that superoxide radicals ($O_2^{\bullet-}$) act as a dominating reactive species in the photodegradation process.

The BiOCl/PANI composites exhibit superior photocatalytic activity to pure PANI and BiOCl under natural sunlight for the photodegradation of Rh-B. There are distinct degradation mechanisms due to the varying molecular structures of dye [39]. During the photocatalyzed mechanism, oxidative species developed on the upper surface of the catalyst, which participated in the decomposition of large dye molecules by forming certain intermediates and, ultimately, transformed them to final products such as CO_2 and H_2O , as demonstrated in Figure 7e. The HOMO and LUMO positions for PANI, as reported in the literature are, 0.8 eV and -1.9 eV, and the conduction band and valence band potentials for BiOCl are reported at around -1.11 eV and 2.10 eV, respectively [50]. BiOCl shows excitation only in the UV region and, due to the broad band gap, it fails to produce photogenerated electron–hole pairs independently in natural light [1]. On the other side, PANI can induce $\pi-\pi^*$ transition after absorption of visible light, resulting in the excitation of photogenerated electrons from HOMO to LUMO orbital. The electron-rich PANI transfers electrons to the conduction band of BiOCl, promoting the reduction of oxygen to generate superoxide radicals as its CB is more negative than the single electron reduction potential (-0.33 eV). The superoxide radicals can further react with water molecules to produce hydroxyl radicals (HO^{\bullet}). Due to the synergic effect, the photogenerated electrons produced by PANI could be directly promoted to the BiOCl conduction band and eventually transferred to the catalyst surface.

As a result, these excited electrons on the catalyst surface react with molecular oxygen and surface water to generate hydroxy (OH^{\bullet}) and superoxide radicals ($O_2^{\bullet-}$), which act as an active oxidative species. These reactive oxidants effectively oxidize Rh-B and convert them to H_2O , CO_2 and other less toxic degraded products. Therefore, BiOCl/PANI photocatalytic performance is greatly increased due to the low recombination rate and rapid separation of electron–hole pairs. The reaction steps involved in the photocatalytic process are given in Equations (3)–(7):





2.12. Reusability Studies

The reusability and stability of photocatalysts play a significant role in practical application. It is necessary to determine the stability of the catalyst over repeated degradation reactions. The photocatalytic activity was tested for the degradation of pollutants for five repeated degradation cycles for 120 min in sunlight, and after every cycle, the photocatalyst was properly cleaned with deionized water and then dried in an oven at 60 °C before the next cycle. It has been observed that the photodegradation efficiency of the catalyst was still 85% after five continuous cycles, which indicates the good stability and reusability of the catalyst. The photocatalytic efficiency was decreased by 12%, as displayed in Figure 8a. The characterization of the BiOCl/PANI composite was conducted before and after degradation. Figure 8b revealed that the sharp peaks in the XRD pattern of PANI/BiOCl after degradation remain unaltered. The surface morphology of the catalyst was not disturbed much, which was confirmed by FESEM analysis, as shown in Figure 8c,d. This suggests the catalyst's high degree of reusability for large-scale applications. The photodegradation of the prepared catalyst was also compared with other studies on photocatalysts, as illustrated in Table 2.

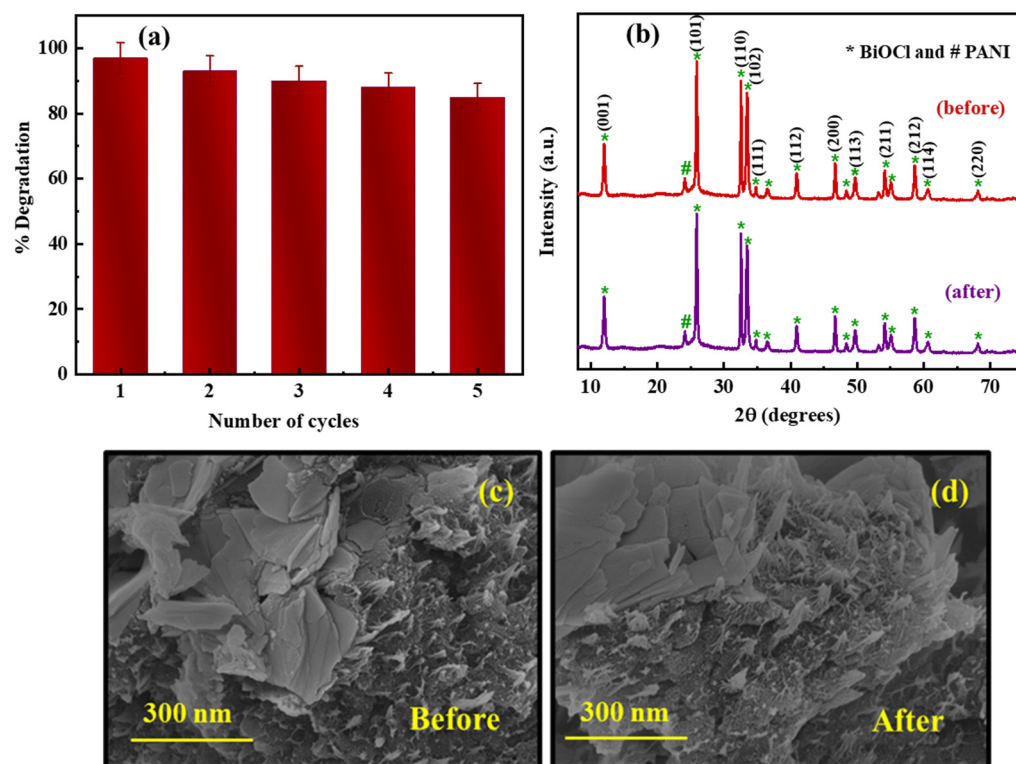


Figure 8. (a) Reusability plot, (b) XRD pattern and (c,d) FESEM images before and after photocatalytic reaction.

Table 2. Comparison of PANI/BiOCl photocatalysts with different reported photocatalysts.

Photocatalyst	Pollutant Degraded (conc.)	Catalyst Concentration (g/L)	Light Source	Time (min)	Degradation Efficiency (%)	Rate Constant (min ⁻¹)	Reference
Au-ZnO	Rh-B (10 ppm)	0.3	Visible	180	78.12	0.0246	[51]
Conjugated polyvinyl chloride/TiO ₂ nanotubes	Rh-B (20 ppb)	0.3	Visible	180	90	0.015	[52]
SnO ₂ /ZnS	Rh-B (5 ppm)	2	Sunlight	100	90	0.046	[53]
β-Bi ₂ O ₃ /g-C ₃ N ₄	TC (10 ppm)	0.5	Visible	N/A	80	0.0311	[54]
Multi wall carbon nanotubes/TiO ₂	TC (10 ppm)	0.2	Visible	100	74	0.064	[14]
Bi ₂ WO ₆ /BiOCl	TC (50 ppm)	N/A	Visible	90	61.5	N/A	[55]
BiOCl/PANI	Rh-B (5 ppm)	0.4	Sunlight	90	97	0.0236	Present work
BiOCl/PANI	TC (10 ppm)	0.5	Sunlight	90	77	0.0106	Present work

3. Experimental Section

3.1. Materials and Chemicals

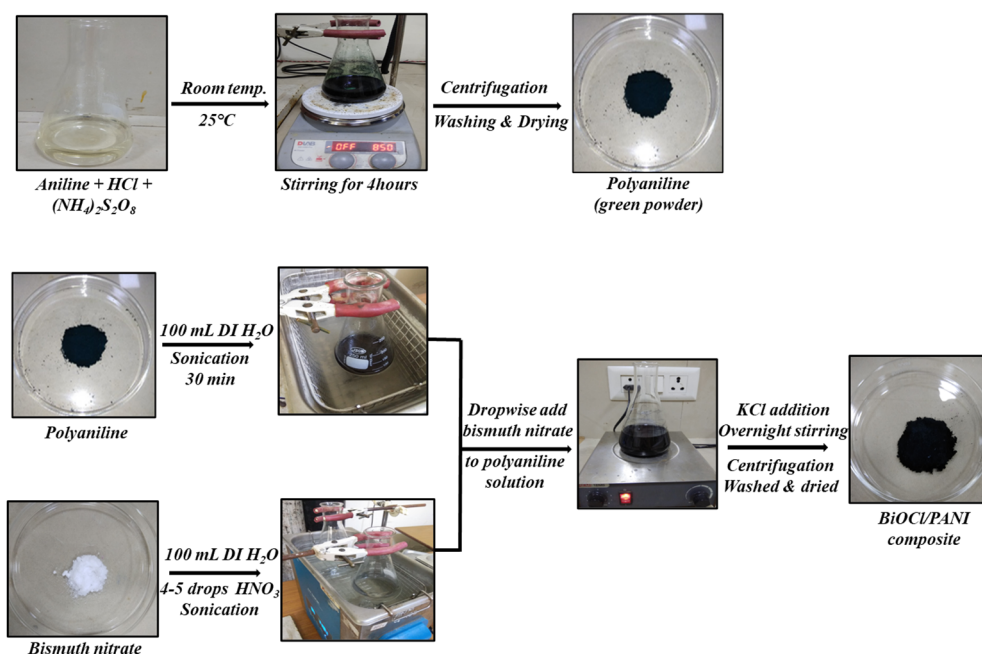
Bismuth nitrate pentahydrate, potassium chloride (KCl), aniline, nitric acid (HNO₃) and hydrochloric acid (HCl) were acquired from Loba Chemie Pvt Ltd, Mumbai, India. Ammonium persulfate (NH₄)₂S₂O₈ was taken from S. D. FINE-CHEM limited (SDFCL), Mumbai, India. Rhodamine-B (Rh-B) dye was also acquired from Loba Chemie Pvt Ltd. and Tetracycline (TC) from Merck, Rahway, NJ, USA. All the chemicals were used in the lab without any further modification and purification. The double-distilled water was employed for solution preparation while performing experiments.

3.2. Synthesis of Polyaniline

To prepare polyaniline, 4.5 mL of aniline was added to 70 mL of hydrochloric acid (HCl) and sonicated the solution for 30 min to obtain a dispersed solution. After 30 min of sonication, 11.5 g of ammonium persulfate (APS) was mixed in 20 mL of distilled water. Dropwise and slow addition of ammonium persulfate was conducted to aniline solution with continuous stirring. The polymerization reaction was allowed to run at 25 °C for 4 h. The resulting reaction mixture was then centrifuged and thoroughly washed with ethanol, deionized water and 2M hydrochloric acid thrice to wash out unreacted material and dried at 60 °C for 24 h to obtain tint green powder of polyaniline [56].

3.3. Synthesis of PANI/BiOCl Composites

Initially, the measured quantity of polyaniline was dispersed in 100 mL of distilled water and then sonicated for half an hour to obtain a dispersed solution. Then, a calculated amount of bismuth nitrate for 5%, 10%, 15%, 20% BiOCl was also dissolved in 100 mL distilled water with 4 to 5 drops of nitric acid (HNO₃) added to it. The resulting bismuth nitrate suspension was added to polyaniline solution, dropwise. Then, the mixture was sonicated for some time and stirred for 15 min and afterward, a measured amount of KCl was added and the whole mixture was stirred overnight. The resulting mixture was then centrifuged and thoroughly washed with deionized water and with ethanol thrice and dried at 60 °C in the oven. By employing this procedure, distinct weight ratios of BiOCl/PANI composite were prepared successfully by varying the amount of PANI, Bi (NO₃)₃.5H₂O and KCl. The pictorial representation of nanocomposites synthesis is illustrated in Scheme 1.



Scheme 1. Real images for the synthesis of PANI and BiOCl/PANI composite.

3.4. Characterization Methods

Nitrogen sorption analysis of the sample was determined by using Microtrac Belsorp Mini-II (Bel, Japan, Inc.). Brunner–Emmet–Teller (BET) method was employed to obtain the specific surface region of material. To avoid the undesirable trapped impurities and gases, the pre-treatment of samples was conducted under N_2 atmosphere for 5–6 h at 120 °C before measurement. Barrett–Joyner–Halenda (BJH) method was employed to achieve the desired pore size distribution. The X-ray diffraction analysis (XRD) of the PANI/BiOCl composite was performed by using PANalytical X-ray diffractometer containing Cu $K\alpha$ radiations ($\lambda = 0.1504$ nm) and using a scan rate of 2° per minute and a 10–90° scan range, operating at 45 kV. For examining the surface morphology of the as-prepared catalyst, ZEISS Field Emission Scanning Electron Microscopy (FESEM) has been used at 5 kV accelerating voltage with Oxford INCA energy dispersive spectrometer (EDS) to obtain the EDX spectra and elemental color mapping. The pH meter was employed to measure and adjust the pH of sample solutions. The photodegradation rate was studied using a UV spectrophotometer (Analytik Jena) (wavelength range of 200 to 800 nm). Photoluminescence spectroscopy (PL) was conducted by employing a PerkinElmer LS-55, USA, PL (excitation wavelength = 340 nm) spectrometer. We used the X-ray photoelectron spectroscopy (XPS) technique to calculate the oxidation state of metal oxides present in the composite with Al $K\alpha$ X-ray radiation origin (1486.7 eV).

3.5. Photocatalytic Study

The photocatalytic performance of the prepared BiOCl/PANI composite was inspected by photodegradation of Rh-B dye and a colorless antibiotic, namely, TC under natural sunlight. To investigate the photodegradation of Rh-B, about 0.4 g/L of the BiOCl/PANI photocatalyst was added to 20 mL of 5 ppm Rh-B aqueous solution, while 0.5 g/L of the photocatalyst was dissolved in 20 mL of 10 ppm TC solution at room temperature. To accomplish the adsorption–desorption equilibrium between photocatalyst surface and noxious pollutant, the solution was constantly stirred in the dark for around half an hour. Then, it was irradiated with solar light for 120 min to achieve the complete degradation of Rh-B and TC. All the experiments were performed in the month of April 2022, under intense sunlight at TIET, Patiala, India. The average solar radiation during the photocatalytic was around 600 W/m^2 , with an average temperature of 29 °C. A UV–Visible spectrometer was used to examine the absorbance spectra of both Rh-B and TC at λ_{max} 555 nm and 360 nm,

respectively, after the complete separation of the BiOCl/PANI catalyst from the resulting solution at regular time intervals. All the degradation experiments were performed in triplicate and error bars in the graph represent the 5% error in the data.

To calculate the degradation efficiency or percent degradation, the Equation (8) was used:

$$\text{Degradation efficiency} = \{(A_0 - A)/A_0\} \times 100 = \{(C_0 - C)/C_0\} \times 100, \quad (8)$$

where A_0 and C_0 represent the initial absorbance of material and the concentration, whereas A and C represent absorbance and concentration at time 't', respectively.

4. Conclusions

The BiOCl/PANI nanocomposite was successfully prepared with different weight ratios of BiOCl (5%, 10%, 15% and 20% BiOCl) by employing a chemisorption technique, which demonstrated remarkable photoactivity for the degradation of Rh-B and colorless pharmaceutical pollutant TC under natural sunlight illumination. The photodegradation results indicate that among all prepared catalysts and TiO₂ P25, the 15% BiOCl/PANI photocatalyst exhibits higher photocatalytic ability for the degradation of Rh-B (97%) and TC (77%). The photocatalyst exhibits a high surface area with favorable optical properties such as low recombination rate and small band gap. Various characterization techniques, such as XRD, FESEM, EDS and XPS analysis, describe the successful formation of the hybrid. The effect of catalyst concentration and the solution pH on degradation was studied. The high degradation efficiency (85%) after five reaction cycles accounted for the good stability of the photocatalyst and was confirmed by XRD and FESEM characterizations. Trapping experiments were performed to determine the dominating active species in the degradation mechanism, and it was evident that superoxide radicals have a major dominating role in the degradation. The synthesized photocatalyst is effective in the photodegradation of model dye and pharmaceutical pollutants in solar light due to its superior properties, which makes it effective for the removal of toxic pollutants accumulating in nature and, in future, it can be substantially used for various wastewater treatments as it is economical, easy to handle and ecosystem friendly.

Supplementary Materials: The following supporting information can be downloaded at: <https://www.mdpi.com/article/10.3390/catal13050795/s1>, Figure S1: Plot of pzc measurement of Rh-B; Table S1: Parameters for Rh-B and TC degradation using different materials.

Author Contributions: Conceptualization, S.S. and S.B.; methodology, S.S., J.G. and S.B.; investigation, J.G.; resources, S.B.; data curation, J.G.; writing—original draft, J.G.; writing—review and editing, S.S. and S.B.; supervision, S.S. and S.B. All authors have read and agreed to the published version of the manuscript.

Funding: This research received no external funding.

Acknowledgments: Janis Goyal would like to thank TIET, Patiala, for providing the instrument facilities and funding. The authors also acknowledge TIET, Patiala, for XRD and FESEM analysis. We are grateful to IIT Delhi for XPS analysis and CeNS Bangalore for HRTEM analysis.

Conflicts of Interest: The authors declare no conflict of interest.

References

1. Sharma, S.; Basu, S.; Shetti, N.P.; Nadagouda, M.N.; Aminabhavi, T.M. Microplastics in the Environment: Occurrence, Perils, and Eradication. *Chem. Eng. J.* **2021**, *408*, 127317. [CrossRef]
2. Sharma, S.; Shetti, N.P.; Basu, S.; Nadagouda, M.N.; Aminabhavi, T.M. Remediation of per- and Polyfluoroalkyls (PFAS) via Electrochemical Methods. *Chem. Eng. J.* **2022**, *430*, 132895. [CrossRef]
3. Sharma, S.; Basu, S.; Shetti, N.P.; Aminabhavi, T.M. Waste-to-Energy Nexus for Circular Economy and Environmental Protection: Recent Trends in Hydrogen Energy. *Sci. Total Environ.* **2020**, *713*, 136633. [CrossRef] [PubMed]
4. Sharma, S.; Basu, S. Visible-Light-Induced Photocatalytic Response of Easily Recoverable Mn₂O₃/SiO₂ Monolith in Centimeter-Scale towards Degradation of Ofloxacin: Performance Evaluation and Product Analysis. *Chemosphere* **2022**, *307*, 135973. [CrossRef]
5. Sharma, S.; Basu, S. Fabrication of Centimeter-Sized Sb₂S₃/SiO₂ Monolithic Mimosa Pudica Nanoflowers for Remediation of Hazardous Pollutants from Industrial Wastewater. *J. Clean. Prod.* **2021**, *280*, 124525. [CrossRef]

6. Cai, Z.; Sun, Y.; Liu, W.; Pan, F.; Sun, P.; Fu, J. An Overview of Nanomaterials Applied for Removing Dyes from Wastewater. *Environ. Sci. Pollut. Res.* **2017**, *24*, 15882–15904. [[CrossRef](#)] [[PubMed](#)]
7. Viswanathan, B. Photocatalytic Degradation of Dyes: An Overview. *Curr. Catal.* **2018**, *7*, 99–121. [[CrossRef](#)]
8. Sharma, S.; Basu, S. Visible-Light-Driven Efficient Photocatalytic Abatement of Recalcitrant Pollutants by Centimeter-Length MoO₃/SiO₂ Monoliths with Long Service Life. *Appl. Mater. Today* **2021**, *23*, 101033. [[CrossRef](#)]
9. Saadati, F.; Keramati, N.; Ghazi, M.M. Influence of Parameters on the Photocatalytic Degradation of Tetracycline in Wastewater: A Review. *Crit. Rev. Environ. Sci. Technol.* **2016**, *46*, 757–782. [[CrossRef](#)]
10. Quesada, H.B.; Baptista, A.T.A.; Cusioli, L.F.; Seibert, D.; de Oliveira Bezerra, C.; Bergamasco, R. Surface Water Pollution by Pharmaceuticals and an Alternative of Removal by Low-Cost Adsorbents: A Review. *Chemosphere* **2019**, *222*, 766–780. [[CrossRef](#)]
11. Singla, S.; Singh, P.; Basu, S.; Devi, P. BiVO₄/MoSe₂ Photocatalyst for the Photocatalytic Abatement of Tetracycline and Photoelectrocatalytic Water Splitting. *Mater. Chem. Phys.* **2023**, *295*, 127111. [[CrossRef](#)]
12. Singla, S.; Basu, S.; Devi, P. Solar Light Responsive 2D/2D BiVO₄/SnS₂ Nanocomposite for Photocatalytic Elimination of Recalcitrant Antibiotics and Photoelectrocatalytic Water Splitting with High Performance. *J. Ind. Eng. Chem.* **2022**, *41*, 101284. [[CrossRef](#)]
13. Qiao, D.; Li, Z.; Duan, J.; He, X. Adsorption and Photocatalytic Degradation Mechanism of Magnetic Graphene oxide/ZnO Nanocomposites for Tetracycline Contaminants. *Chem. Eng. J.* **2020**, *400*, 125952. [[CrossRef](#)]
14. Ahmadi, M.; Ramezani Motlagh, H.; Jaafarzadeh, N.; Mostoufi, A.; Saeedi, R.; Barzegar, G.; Jorfi, S. Enhanced Photocatalytic Degradation of Tetracycline and Real Pharmaceutical Wastewater Using MWCNT/TiO₂ Nano-Composite. *J. Environ. Manage.* **2017**, *186*, 55–63. [[CrossRef](#)]
15. Singla, S.; Sharma, S.; Basu, S. MoS₂/WO₃ Heterojunction with the Intensified Photocatalytic Performance for Decomposition of Organic Pollutants under the Broad Array of Solar Light. *J. Clean. Prod.* **2021**, *324*, 129290. [[CrossRef](#)]
16. Chatterjee, M.J.; Ahamed, S.T.; Mitra, M.; Kulsi, C.; Mondal, A.; Banerjee, D. Visible-Light Influenced Photocatalytic Activity of Polyaniline -Bismuth Selenide Composites for the Degradation of Methyl Orange, Rhodamine B and Malachite Green Dyes. *Appl. Surf. Sci.* **2019**, *470*, 472–483. [[CrossRef](#)]
17. Sharma, S.; Basu, S. Construction of an Efficient and Durable Hierarchical Porous CuO/SiO₂ Monolith for Synergistically Boosting the Visible-Light-Driven Degradation of Organic Pollutants. *Sep. Purif. Technol.* **2021**, *279*, 119759. [[CrossRef](#)]
18. Dashairya, L.; Sharma, S.; Rath, A.; Saha, P.; Basu, S. Solar-Light-Driven Photocatalysis by Sb₂S₃/carbon Based Composites towards Degradation of Noxious Organic Pollutants. *Mater. Chem. Phys.* **2021**, *273*, 125120. [[CrossRef](#)]
19. Monga, D.; Sharma, S.; Shetti, N.P.; Basu, S.; Reddy, K.R.; Aminabhavi, T.M. Advances in Transition Metal Dichalcogenide-Based Two-Dimensional Nanomaterials. *Mater. Today Chem.* **2021**, *19*, 100399. [[CrossRef](#)]
20. Sharma, S.; Basu, S. Highly Reusable Visible Light Active Hierarchical Porous WO₃/SiO₂ Monolith in Centimeter Length Scale for Enhanced Photocatalytic Degradation of Toxic Pollutants. *Sep. Purif. Technol.* **2020**, *231*, 115916. [[CrossRef](#)]
21. Zhang, Y.; Gao, J.; Xin, X.; Wang, L.; Li, H.; Zheng, X.; Jiang, Y. Immobilization Laccase on Heterophase TiO₂ Microsphere as a Photo-Enzyme Integrated Catalyst for Emerging Contaminants Degradation under Visible Light. *Appl. Mater. Today* **2020**, *21*, 100810. [[CrossRef](#)]
22. Kundu, A.; Sharma, S.; Basu, S. Modulated BiOCl Nanoplates with Porous G-C₃N₄ Nanosheets for Photocatalytic Degradation of Color/colorless Pollutants in Natural Sunlight. *J. Phys. Chem. Solids* **2021**, *154*, 110064. [[CrossRef](#)]
23. Dong, S.; Feng, J.; Fan, M.; Pi, Y.; Hu, L.; Han, X.; Liu, M.; Sun, J.; Sun, J. Recent Developments in Heterogeneous Photocatalytic Water Treatment Using Visible Light-Responsive Photocatalysts: A Review. *RSC Adv.* **2015**, *5*, 14610–14630. [[CrossRef](#)]
24. Singh, J.; Sharma, S.; Aanchal; Basu, S. Synthesis of Fe₂O₃/TiO₂ Monoliths for the Enhanced Degradation of Industrial Dye and Pesticide via Photo-Fenton Catalysis. *J. Photochem. Photobiol. A Chem.* **2019**, *376*, 32–42. [[CrossRef](#)]
25. Zarezaadeh, S.; Habibi-Yangjeh, A.; Mousavi, M. BiOBr and AgBr Co-Modified ZnO Photocatalyst: A Novel Nanocomposite with P-N-N Heterojunctions for Highly Effective Photocatalytic Removal of Organic Contaminants. *J. Photochem. Photobiol. A Chem.* **2019**, *379*, 11–23. [[CrossRef](#)]
26. Rafiq, A.; Ikram, M.; Ali, S.; Niaz, F.; Khan, M.; Khan, Q.; Maqbool, M. Photocatalytic Degradation of Dyes Using Semiconductor Photocatalysts to Clean Industrial Water Pollution. *J. Ind. Eng. Chem.* **2021**, *97*, 111–128. [[CrossRef](#)]
27. Zhang, D.; Su, C.; Yao, S.; Li, H.; Pu, X.; Geng, Y. Facile in Situ Chemical Transformation Synthesis, Boosted Charge Separation, and Increased Photocatalytic Activity of BiPO₄/BiOCl P-N Heterojunction Photocatalysts under Simulated Sunlight Irradiation. *J. Phys. Chem. Solids* **2020**, *147*, 109630. [[CrossRef](#)]
28. Xu, Z.; Zhang, C.; Zhang, Y.; Gu, Y.; An, Y. BiOCl-Based Photocatalysts: Synthesis Methods, Structure, Property, Application, and Perspective. *Inorg. Chem. Commun.* **2022**, *138*, 109277. [[CrossRef](#)]
29. Monga, D.; Basu, S. Single-Crystalline 2D BiOCl Nanorods Decorated with 2D MoS₂ Nanosheets for Visible Light-Driven Photocatalytic Detoxification of Organic and Inorganic Pollutants. *FlatChem* **2021**, *28*, 100267. [[CrossRef](#)]
30. Lee, S.; Chang, C.-J. Recent Developments about Conductive Polymer Based Composite Photocatalysts. *Polymers* **2019**, *11*, 206. [[CrossRef](#)]
31. Taghizadeh, A.; Taghizadeh, M.; Jouyandeh, M.; Yazdi, M.K.; Zarrintaj, P.; Saeb, M.R.; Lima, E.C.; Gupta, V.K. Conductive Polymers in Water Treatment: A Review. *J. Mol. Liq.* **2020**, *312*, 113447. [[CrossRef](#)]
32. Park, Y.; Numan, A.; Ponomarev, N.; Iqbal, J.; Khalid, M. Enhanced Photocatalytic Performance of PANI-rGO-MnO₂ Ternary Composite for Degradation of Organic Contaminants under Visible Light. *J. Environ. Chem. Eng.* **2021**, *9*, 106006. [[CrossRef](#)]

33. Yadav, A.; Kumar, H.; Sharma, R.; Kumari, R. Influence of Polyaniline on the Photocatalytic Properties of Metal Nanocomposites: A Review. *Colloid Interface Sci. Commun.* **2021**, *40*, 100339. [[CrossRef](#)]
34. Tang, M.; Li, X.; Deng, F.; Han, L.; Xie, Y.; Huang, J.; Chen, Z.; Feng, Z.; Zhou, Y. BiPO₄/Ov-BiOBr High-Low Junctions for Efficient Visible Light Photocatalytic Performance for Tetracycline Degradation and H₂O₂ Production. *Catalysts* **2023**, *13*, 634. [[CrossRef](#)]
35. Xie, L.; Wu, P.; Lei, Q.; Xu, C.; Huang, W.; Chen, X.; Yang, K.; He, H. Constructing Z-Scheme 0D/2D TiO₂ Nanoparticles/Bi₂O₃ Nanosheet Heterojunctions with Enhanced Visible Light Induced Photocatalytic Antibiotics Degradation and Hydrogen Evolution. *Catalysts* **2023**, *13*, 583. [[CrossRef](#)]
36. Al-Musawi, T.J.; Yilmaz, M.; Ramírez-Coronel, A.A.; Al-Awsi, G.R.L.; Alwaily, E.R.; Asghari, A.; Balarak, D. Degradation of Amoxicillin under a UV or Visible Light Photocatalytic Treatment Process Using Fe₂O₃/bentonite/TiO₂: Performance, Kinetic, Degradation Pathway, Energy Consumption, and Toxicology Studies. *Optik* **2023**, *272*, 170230. [[CrossRef](#)]
37. Chen, R.; Ding, S.; Fu, N.; Ren, X. Preparation of a G-C₃N₄/Ag₃PO₄ Composite Z-Type Photocatalyst and Photocatalytic Degradation of Ofloxacin: Degradation Performance, Reaction Mechanism, Degradation Pathway and Toxicity Evaluation. *J. Environ. Chem. Eng.* **2023**, *11*, 109440. [[CrossRef](#)]
38. Tanwar, R.; Kumar, S.; Mandal, U.K. Photocatalytic Activity of PANI/Fe₀ Doped BiOCl under Visible Light-Degradation of Congo Red Dye. *J. Photochem. Photobiol. A Chem.* **2017**, *333*, 105–116. [[CrossRef](#)]
39. Wang, Q.; Hui, J.; Li, J.; Cai, Y.; Yin, S.; Wang, F.; Su, B. Photodegradation of Methyl Orange with PANI-Modified BiOCl Photocatalyst under Visible Light Irradiation. *Appl. Surf. Sci.* **2013**, *283*, 577–583. [[CrossRef](#)]
40. Wang, J.; Hao, X.; Jiang, Y.; Zhang, D.; Ren, L.; Gong, J.; Wu, X.; Zhang, Y.; Tong, Z. Synthesis, Structure, and Photocatalytic Activity of PANI/BiOCl Nanocomposites. *Mater. Res. Express* **2019**, *6*, 0850c1. [[CrossRef](#)]
41. Luo, Y.; Huang, Q.; Li, B.; Dong, L.; Fan, M.; Zhang, F. Synthesis and Characterization of Cu₂O-modified Bi₂O₃ Nanospheres with Enhanced Visible Light Photocatalytic Activity. *Appl. Surf. Sci.* **2015**, *357*, 1072–1079. [[CrossRef](#)]
42. Cui, J.; Tao, S.; Yang, X.; Yu, X.; Sun, S.; Yang, Q.; Wei, W.; Liang, S. Facile Construction of Nickel-Doped Hierarchical BiOCl Architectures for Enhanced Visible-Light-Driven Photocatalytic Activities. *Mater. Res. Bull.* **2021**, *138*, 111208. [[CrossRef](#)]
43. Zhang, Z.; Jiang, Y.; Chi, M.; Yang, Z.; Nie, G.; Lu, X.; Wang, C. Fabrication of Au Nanoparticles Supported on CoFe₂O₄ Nanotubes by Polyaniline Assisted Self-Assembly Strategy and Their Magnetically Recoverable Catalytic Properties. *Appl. Surf. Sci.* **2016**, *363*, 578–585. [[CrossRef](#)]
44. Tanwar, R.; Mandal, U.K. Photocatalytic Activity of Ni_{0.5}Zn_{0.5}Fe₂O₄@polyaniline Decorated BiOCl for Azo Dye Degradation under Visible Light—Integrated Role and Degradation Kinetics Interpretation. *RSC Adv.* **2019**, *9*, 8977–8993. [[CrossRef](#)] [[PubMed](#)]
45. Namdarian, A.; Goljanian Tabrizi, A.; Arsalani, N.; Khataee, A.; Mohammadi, A. Synthesis of PANi Nanoarrays Anchored on 2D BiOCl Nanoplates for Photodegradation of Congo Red in Visible Light Region. *J. Ind. Eng. Chem.* **2020**, *81*, 228–236. [[CrossRef](#)]
46. Yaghoubi-berijani, M.; Bahramian, B. Preparation and Measurement of Properties of BiOBr/BiOCl/PANI Ternary Nanocomposite for Highly Efficient Visible Light Photocatalytic Applications. *Res. Chem. Intermed.* **2021**, *47*, 2311–2330. [[CrossRef](#)]
47. Monga, D.; Basu, S. Combination of MoS₂ Nanopetals with Ag Nanoparticles Decorated Graphene Oxide for Boosting Photocatalytic Abatement of Recalcitrant Pollutants under Visible Light Irradiation. *Adv. Powder Technol.* **2022**, *33*, 103555. [[CrossRef](#)]
48. Dai, W.; Jiang, L.; Wang, J.; Pu, Y.; Zhu, Y.; Wang, Y.; Xiao, B. Efficient and Stable Photocatalytic Degradation of Tetracycline Wastewater by 3D Polyaniline/Perylene Diimide Organic Heterojunction under Visible Light Irradiation. *Chem. Eng. J.* **2020**, *397*, 125476. [[CrossRef](#)]
49. Xu, Y.; Ma, Y.; Ji, X.; Huang, S.; Xia, J.; Xie, M.; Yan, J.; Xu, H.; Li, H. Conjugated Conducting Polymers PANI Decorated Bi₁₂O₁₇Cl₂ Photocatalyst with Extended Light Response Range and Enhanced Photoactivity. *Appl. Surf. Sci.* **2019**, *464*, 552–561. [[CrossRef](#)]
50. Bouziani, A.; Yahya, M.; Bianchi, C.L.; Falletta, E.; Celik, G. Ternary Polyaniline@Bi₂O₃-BiOCl Nanocomposites as Innovative Highly Active Photocatalysts for the Removal of the Dye under Solar Light Irradiation. *Nanomaterials* **2023**, *13*, 713. [[CrossRef](#)]
51. Ahmad, M.; Rehman, W.; Khan, M.M.; Qureshi, M.T.; Gul, A.; Haq, S.; Ullah, R.; Rab, A.; Mena, F. Phytogenic Fabrication of ZnO and Gold Decorated ZnO Nanoparticles for Photocatalytic Degradation of Rhodamine B. *J. Environ. Chem. Eng.* **2021**, *9*, 104725. [[CrossRef](#)]
52. Bui, D.P.; Huu Pham, H.; Minh Cao, T.; Van Pham, V. Preparation of Conjugated Polyvinyl chloride/TiO₂ Nanotubes for Rhodamine B Photocatalytic Degradation under Visible Light. *J. Chem. Technol. Biotechnol.* **2020**, *95*, 2707–2714. [[CrossRef](#)]
53. Hu, L.; Chen, F.; Hu, P.; Zou, L.; Hu, X. Hydrothermal Synthesis of SnO₂/ZnS Nanocomposite as a Photocatalyst for Degradation of Rhodamine B under Simulated and Natural Sunlight. *J. Mol. Catal. A Chem.* **2016**, *411*, 203–213. [[CrossRef](#)]
54. Hong, Y.; Li, C.; Yin, B.; Li, D.; Zhang, Z.; Mao, B.; Fan, W.; Gu, W.; Shi, W. Promoting Visible-Light-Induced Photocatalytic Degradation of Tetracycline by an Efficient and Stable Beta-Bi₂O₃@g-C₃N₄ Core/shell Nanocomposite. *Chem. Eng. J.* **2018**, *338*, 137–146. [[CrossRef](#)]
55. Liang, Z.; Zhou, C.; Yang, J.; Mo, Q.; Zhang, Y.; Tang, Y. Visible Light Responsive Bi₂WO₆/BiOCl Heterojunction with Enhanced Photocatalytic Activity for Degradation of Tetracycline and Rhodamine B. *Inorg. Chem. Commun.* **2018**, *93*, 136–139. [[CrossRef](#)]
56. Kumar, A.; Kumar, R.; Pandey, G. Synthesis, Characterization of Titania/Polyaniline/GO Nanocomposites, and Its Photocatalytic Activity under UV-Visible Light. *Macromol. Symp.* **2018**, *379*, 1600192. [[CrossRef](#)]

Disclaimer/Publisher's Note: The statements, opinions and data contained in all publications are solely those of the individual author(s) and contributor(s) and not of MDPI and/or the editor(s). MDPI and/or the editor(s) disclaim responsibility for any injury to people or property resulting from any ideas, methods, instructions or products referred to in the content.